Journal of Engineering Science and Technology
Vol. 21, No. 4 (2026) 1089 - 1108

CALCIUM COPPER TITANATE (CCTO) – POLYDIMETHYLSILOXANE (PDMS) COMPOSITES FOR FLEXIBLE MICROSTRIP ANTENNA SUBSTRATES

ROSLIN ATHIRAH ROSLAN[1], NURUL HAZLINA NOORDIN[1,2,*], NURULFADZILAH HASAN[1], NOOR ZIRWARTUL AHLAM BINTI NAHARUDDIN[1], NOR HADZFIZAH MOHD RADI[1]

[1]Faculty of Electrical and Electronic Engineering Technology, Universiti Malaysia Pahang Al-Sultan Abdullah (UMPSA), Malaysia
[2]UMPSA STEM Lab, Faculty of Electrical and Electronic Engineering Technology, Universiti Malaysia Pahang Al-Sultan Abdullah (UMPSA), Malaysia
*Corresponding author: hazlina@umpsa.edu.my

Abstract

This study examines calcium copper titanate (CCTO)–polydimethylsiloxane (PDMS) composites fabricated via a solvent-assisted dispersion route, with emphasis on their dielectric performance for high-frequency applications. Composites containing 10–60 wt.% CCTO were prepared using isopropanol (IPA) to promote uniform filler distribution within the polymer matrix. Morphological and chemical analyses by scanning electron microscopy (SEM), energy-dispersive X-ray spectroscopy (EDX), and Fourier-transform infrared spectroscopy (FTIR) confirmed homogeneous microstructure and physical filler–matrix interactions. Broadband dielectric measurements across 1–10 GHz revealed that the composites maintained stable permittivity with controllable dielectric loss. At 60 wt.% loading, the composite achieved a dielectric constant of 5.84, a loss tangent of 0.20, and an electrical conductivity of 0.066 S/m at 7.5 GHz. The ability to sustain high permittivity with moderate losses in the GHz range represents the novelty of this work, demonstrating the suitability of CCTO–PDMS composites as promising substrates for wearable sensors, conformal RF devices, and compact flexible antennas. Unlike many polymer–ceramic composites characterized primarily at low frequencies, this work demonstrates stable dielectric behaviour in the GHz range. The frequency-stable performance achieved through solvent-assisted dispersion highlights the potential of CCTO–PDMS composites as flexible substrates for wearable sensors, conformal RF devices, and compact microwave antennas.

Keywords: CCTO, Composite, Dielectric, Flexible substrate, PDMS.

1. Introduction

The advancement of flexible and wearable electronics has accelerated the demand for high-performance dielectric materials with both mechanical compliance and frequency stability [1-5]. Flexible electronics are expected to revolutionize consumer electronics, medical devices, and aerospace systems by providing lightweight, durable, and adaptable solutions. A key challenge is balancing dielectric performance with flexibility.

Ceramic materials such as calcium copper titanate ($CaCu_3Ti_4O_{12}$, CCTO) are known for their exceptionally high dielectric constants but are brittle and lack flexibility [6-8]. In contrast, polymers such as polydimethylsiloxane (PDMS) provide excellent elasticity, transparency, and chemical resistance but have inherently low dielectric constants, limiting their application in high-frequency or miniaturized systems [9, 10]. Recent studies have shown that incorporating high-permittivity ceramics into flexible matrices offers a promising pathway to combine the advantages of both materials [11-13]. For example, CCTO-based composites have been explored in capacitors, microstrip antennas, energy harvesters, and flexible sensors [14-18].

Although significant progress has been achieved, uniform dispersion and strong filler–matrix interaction remain difficult to obtain. Poor dispersion often results in agglomeration, stress concentrations, and inconsistent dielectric properties. Poor dispersion leads to agglomeration, stress concentrations, and inconsistent dielectric properties. Solvent-assisted techniques have been used to improve particle dispersion, but they introduce challenges related to solvent removal, environmental safety, and processing complexity [19, 20].

Wang et al. [21], reported that silane-modified CCTO nanoparticles dispersed through an ethanol/THF route exhibited improved microstructural uniformity and enhanced permittivity and another study, Liu et al. [22] incorporated CCTO@MWCNT hybrids into PDMS, obtaining a dielectric constant exceeding 2000 at 1 kHz, although the investigation remained confined to the low-frequency regime. These works underscore the effectiveness of solvent-assisted fabrication and hybrid filler strategies in improving dispersion and dielectric response, but they also highlight the prevailing emphasis on low-frequency characterization rather than broadband GHz performance.

Despite these advances, important limitations remain. Most reported studies confine dielectric measurements to the Hz–kHz range, which does not capture the dispersion and loss mechanisms relevant at microwave frequencies. Moreover, much of the existing literature prioritizes permittivity enhancement, with less attention given to dielectric loss and conductivity parameters that are critical for the design of practical RF and microwave devices. Furthermore, only a few studies attempt to systematically link microstructural observations obtained by SEM and EDX, or chemical insights from FTIR, with broadband dielectric behaviour.

The absence of high-frequency investigations represents a clear gap in the field. Although solvent-assisted methods have demonstrated improved dispersion, their impact on the GHz-range dielectric performance of CCTO–PDMS composites have not yet been addressed. This study responds to that gap by combining morphological, chemical, and broadband dielectric characterization of solvent-fabricated composites with ceramic loadings up to 60 wt.%. By demonstrating

stable permittivity with controlled dielectric losses in the 1–10 GHz range, it establishes the processing–property relationship for solvent-processed CCTO–PDMS systems and confirms their potential as flexible substrates for wearable sensors, conformal RF devices, and compact antennas.

A solvent-assisted dispersion method was employed to fabricate the CCTO–PDMS composites in order to promote uniform distribution of ceramic particles within the polymer matrix. The use of a solvent such as isopropanol helps to temporarily reduce the viscosity of the PDMS precursor, allowing CCTO particles to disperse more effectively before curing. This approach is commonly adopted in polymer–ceramic composite preparation to minimize particle clustering and to improve filler–matrix interaction. In this work, it is assumed that the solvent evaporates completely during the mixing and curing stages, resulting in a stable two-phase composite consisting of CCTO fillers embedded within the PDMS matrix. However, several limitations should be considered. At higher filler loadings, partial agglomeration of ceramic particles may still occur despite solvent-assisted mixing, which can influence the uniformity of the dielectric response. In addition, incomplete dispersion or residual solvent traces may slightly affect the microstructure and dielectric performance. Therefore, careful mixing, solvent evaporation, and curing conditions were applied to ensure reproducible composite formation.

2. Materials and Methods

2.1. Materials

The materials used in this study were Sylgard™ 184 silicone elastomer (Dow Corning, USA), calcium copper titanate ($CaCu_3Ti_4O_{12}$, CCTO) powder, and isopropanol (IPA). The CCTO powder was purchased from Nanografi Nanotechnology Inc. (Ankara, Türkiye), a commercial supplier specializing in high-purity functional ceramics. According to the manufacturer's data, the powder has an average particle size of about 360 nm, 99.5 % purity, and a density of 4.9 g cm^{-3}. The polymer matrix consisted of Sylgard™ 184 PDMS supplied by Dow Corning (USA), a two-component silicone elastomer kit containing a base and curing agent, mixed in a 10:1 weight ratio as recommended by the manufacturer. The Sylgard base has a density of 1.03 g cm^{-3} and provides excellent elasticity and chemical stability for dielectric composite fabrication. Isopropanol (≥ 99.8 % purity, Sigma-Aldrich, USA) was used as a dispersing solvent to promote uniform particle distribution within the PDMS matrix. All materials were used as received without further purification.

2.2. Elemental composition analysis of CCTO nanopowder

The chemical composition of the purchased $CaCu_3Ti_4O_{12}$ (CCTO) nanopowder (Nanografi, USA) was examined using energy-dispersive X-ray spectroscopy (EDX) to verify the stoichiometry and material purity. The analysis was performed at an accelerating voltage of 10 kV under high-vacuum conditions.

The chemical composition of the purchased $CaCu_3Ti_4O_{12}$ powder was examined using EDX to verify stoichiometry and purity. The measured elemental ratios, as shown in Table 1**,** (Ca = 5.6A at%, Cu = 12.4 at%, Ti = 24.4 at%, O = 57.6 at%), closely matched the theoretical stoichiometry (Ca = 5.0 at%, Cu = 15.0 at%, Ti = 20.0 at%, O = 60.0 at%). The close agreement between the experimental atomic

percentages and theoretical ratios confirms that the as received nanopowder is essentially stoichiometric and of high purity, thereby validating its suitability as a dielectric filler in this study.

Table 1. Comparison of measured elemental composition of CCTO nanopowder (Nanografi, USA) with theoretical stoichiometry based on atomic percentage.

Element	Theoretical (%Atoms)	Measured (Atom %)
Ca	5	5.60±0.52
Cu	15	12.36±0.51
Ti	20	24.42±1.27
0	60	57.62±1.67

2.3. Sample preparation

CCTO loadings ranging from 10 to 60 wt.% were selected to evaluate the influence of filler concentration on dielectric performance while maintaining the structural integrity and flexibility of the PDMS matrix. Preliminary trials at higher loadings (70–80 wt.%) resulted in incomplete curing and poor structural stability, likely due to insufficient polymer continuity and hindered crosslinking. Therefore, 60 wt.% was considered the practical upper limit for producing fully cured and uniform composites.

CCTO–PDMS composites were fabricated with ceramic filler loadings of 10 wt,%, 20 wt.%, 40wt.%, and 60wt.% by weight. Nanosized CCTO powder was first weighed using a precision digital scale and dispersed in isopropanol to aid particle separation. The suspension was then sonicated for 5 minutes in a bath sonicator to improve dispersion and minimize agglomeration. The sonication process employed a Branson 1800 bath sonicator (40 kHz, 70 W), and the 5-minute duration was optimized to minimize particle agglomeration while avoiding thermal degradation of IPA.

Next, the PDMS base resin (Sylgard 184 Part A) was added directly into the beaker containing the CCTO–IPA mixture. The blend was stirred using a magnetic hotplate stirrer (IKA C-MAG HS7) at 85 °C, set to speed level 1, and mixed continuously for 8 hours. This step ensured homogeneous mixing and gradual evaporation of the solvent while minimizing bubble formation. Once the solvent had fully evaporated, the curing agent (Part B) was added at a ratio of 1:10 (9.09 wt.%), as recommended. This curing ratio is known to improve elasticity and enhance mechanical strength prior to material failure. The final mixture was gently stirred to avoid air entrapment, then cast into clean silicone moulds and left to cure at room temperature for 24 hours. The curing was conducted at 25 ± 2 °C and ambient humidity of 60–70%, ensuring optimal polymer crosslinking and avoiding moisture-related defects in the matrix. This process was consistently repeated for all filler concentrations to ensure uniformity across samples.

2.4. Characterization

The composites were characterized by:

- SEM (Hitachi SU3500) for morphology, with EDX mapping for elemental confirmation.

- FTIR (Nicolet iS50) in the range 400–4000 cm^{-1} to investigate filler–matrix interactions.
- Dielectric properties measured using a SPEAG dielectric probe connected to a Rohde & Schwarz ZVB20 vector network analyser across 1–10 GHz.
- Four independent samples per filler loading were tested, and five repeated measurements were averaged to assess reproducibility, with standard deviations reported (<5%).

The surface morphology of CCTO–PDMS composites was examined using Scanning Electron Microscopy (SEM, Hitachi SU3500) at ×3,000 magnification, 10 kV landing voltage, and 10.1 mm working distance. Samples were gold-coated to reduce charging, and five regions per sample were imaged under high vacuum to ensure representative microstructural analysis. Quantitative image analysis was subsequently performed using ImageJ software to evaluate agglomerate size and particle distribution. For each composition, three representative SEM micrographs acquired at identical magnification were analysed. The images were converted to grayscale (8-bit), and a consistent thresholding protocol was applied to segment ceramic particles from the PDMS matrix. A minimum particle area filter was introduced to eliminate background noise and artefacts. Agglomerate size was determined using Feret's diameter, and the area fraction was calculated to estimate the relative ceramic coverage within the matrix. The reported values correspond to the mean of three independent measurements for each filler concentration.

Dielectric properties were measured using a SPEAG 3.5 probe connected to a ZVB20 vector network analyser, across 1–10 GHz at room temperature, with five measurements taken for each sample to obtain an average value. As shown in Fig. 1, the dielectric measurement setup comprises a vector network analyser, a dielectric probe, and an adjustable stage for the material under test (MUT). Complementary to the morphological study, Fourier transform infrared spectroscopy (FTIR, Nicolet iS50) was employed to investigate the chemical bonding and functional groups within the composites. Spectra were recorded in the range of 400–4000 cm^{-1} to identify characteristic absorption bands associated with both the PDMS polymer matrix and the CCTO ceramic filler.

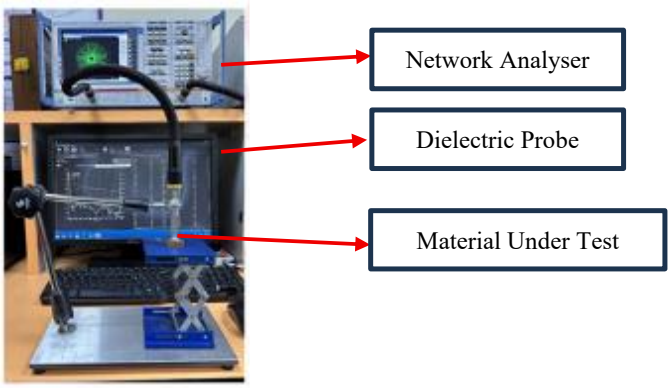

Fig. 1. Dielectric measurement setup comprising a vector network analyser, dielectric probe, and adjustable stage for the material under test (MUT).

2.5. Mixing/prediction method

To predict the effective dielectric response of CCTO–PDMS composites, several classical and semi-empirical models were considered. These models relate the effective dielectric permittivity (ε_c) of a composite to the intrinsic permittivity of the matrix (ε_m), the filler (ε_f), and the filler volume fraction (ϕ). Each model carries specific assumptions regarding microstructural configuration, particle geometry, and interfacial interactions.

The Wiener model establishes theoretical upper and lower limits based on series and parallel arrangements of the filler and matrix [23]. This model does not capture interfacial or morphological effects, however, it provides the physical boundary within which all practical models must fall, as shown in Eq. (1) [24].

$$\varepsilon_{\text{upper}} = \phi\varepsilon_f + (1-\phi)\varepsilon_m, \quad \varepsilon_{\text{lower}} = \left[\frac{\phi}{\varepsilon_f} + \frac{(1-\phi)}{\varepsilon_m}\right]^{-1} \tag{1}$$

The logarithmic mixture rule, shown in Eq. (2) [23], assumes exponential scaling of dielectric properties with volume fraction. It is often used as an empirical fit for composites with heterogeneous filler dispersion [25].

$$\ln \varepsilon_c = \phi \ln \varepsilon_f + (1-\phi)\varepsilon_m \tag{2}$$

The Maxwell-Garnett model is derived for systems where spherical filler particles are embedded in a continuous host matrix. It accounts for the polarization of isolated inclusions and their local field interactions with the surrounding medium, as given in Eq. (3) [26].

$$\varepsilon_c = \varepsilon_m \left[\frac{\varepsilon_f + 2\varepsilon_m + 2\phi(\varepsilon_f - \varepsilon_m)}{\varepsilon_f + 2\varepsilon_m - \phi(\varepsilon_f - \varepsilon_m)}\right] \tag{3}$$

This model is most valid at low-to-moderate filler loadings, where the filler particles remain well dispersed and interparticle coupling is minimal [27]. Given the elastomeric nature of PDMS and the relatively moderate dielectric contrast with CCTO, the Maxwell–Garnett formulation is expected to capture the effective permittivity trends accurately.

The Jayasundere–Smith model modifies the Maxwell–Garnett relation by incorporating interaction terms between filler particles [28]. It becomes more relevant as the filler content increases and particle clustering begins to affect the effective dielectric constant, as given in Eq. (4) [29].

$$\varepsilon_c = \varepsilon_m \left[\frac{1 + 3\phi\left[\frac{(\varepsilon_f - \varepsilon_m)}{\varepsilon_f + 2\varepsilon_m)}\right]}{1 - \phi\left[\frac{(\varepsilon_f - \varepsilon_m)}{\varepsilon_f + 2\varepsilon_m)}\right]}\right] \tag{4}$$

The Bruggeman model symmetrically treats both matrix and filler phases, shown in Eq. (5), making it particularly suitable for composites with higher filler loadings where neither phase can be considered continuous [30, 31].

$$\phi \frac{\varepsilon_f - \varepsilon_c}{\varepsilon_f + 2\varepsilon_c} + (1-\phi) \frac{\varepsilon_m - \varepsilon_c}{\varepsilon_m + 2\varepsilon_c} = 0 \tag{5}$$

In this work, all five models were applied to estimate the dielectric permittivity of CCTO–PDMS composites across filler loadings ranging from 10 to 60 wt.%. The predicted values were compared with experimentally measured permittivity at 5.2 GHz.

2.6. Composite Labelling and Thickness Control

Each composite sample was labelled according to the weight percentage of CCTO filler (CCTO 10%, CCTO 20%, CCTO 40%, and CCTO 60%). The final cured composites were trimmed to uniform thicknesses of approximately 1.0 mm using a precision blade and thickness gauge to ensure consistency across dielectric measurements. Dimensional accuracy was confirmed with a digital calliper (±0.01 mm resolution). For each filler composition, four independent samples were prepared and characterized to ensure repeatability and statistical significance in the measurements. Standard deviations were calculated for the dielectric values.

3. Result and Discussion

3.1. Morphological and Elemental Characterization

The surface morphology of PDMS–CCTO composites was examined using SEM, as shown in Fig. 2. At 10 wt.% and 20 wt.% CCTO loadings, the particles are relatively well dispersed within the PDMS matrix, with minimal visible agglomeration. As the filler content increases to 40 wt.% and 60 wt.%, localized particle clustering becomes more evident, particularly at 60 wt.%, where larger agglomerated regions are observed. This morphological evolution suggests that increasing ceramic loading reduces interparticle spacing, thereby enhancing particle–particle interaction within the polymer matrix.

Across all samples, the surfaces remain relatively smooth, indicating effective embedding of ceramic fillers within the PDMS host. However, increased clustering at 40 wt.% and especially at 60 wt.% implies reduced dispersion efficiency at higher filler concentrations. The formation of such clusters reflects stronger interparticle interaction, which may influence structural homogeneity and dielectric uniformity of the composite. In contrast, the 10 wt.% sample exhibits more uniform dispersion with fewer visible agglomerates. These observations provide insight into how filler loading governs internal structural organization, which is critical for RF substrate applications.

To substantiate the qualitative observations, quantitative image analysis was performed using ImageJ software on three representative SEM micrographs for each composition. A consistent thresholding procedure and minimum particle area filter were applied to ensure reliable segmentation and comparability across samples. Agglomerate size was quantified using Feret's diameter, while the area fraction was determined to estimate the relative ceramic coverage within the matrix. The quantitative results are summarized in Table 2.

The mean agglomerate diameter was approximately 0.51 μm at 10 wt.%, decreased to 0.43 μm at 20 wt.%, and subsequently increased to 0.46 μm and 0.53 μm at 40 wt.% and 60 wt.%, respectively. The slightly higher value at 10 wt.% compared to 20 wt.% may be attributed to the presence of isolated local clusters at low filler concentration, where limited particle–particle interaction can lead to non-uniform initial dispersion. At intermediate loading (20 wt.%), improved mixing efficiency and enhanced shear interaction during processing may promote more homogeneous particle distribution, resulting in a reduction in average agglomerate size. As the filler content increases further, reduced interparticle spacing facilitates progressive particle coalescence, leading to larger agglomerates at 60 wt.%.

Importantly, the microstructural evolution at 60 wt.% correlates with the enhanced dielectric permittivity reported for this composition. Reduced interparticle spacing and intensified particle interaction promote stronger interfacial polarization, contributing to the elevated effective permittivity. While moderate clustering may enhance polarization effects, excessive agglomeration can introduce local electric field heterogeneity and influence dielectric loss behaviour. Therefore, achieving an optimal balance between dispersion uniformity and filler connectivity is essential for maximizing dielectric performance.

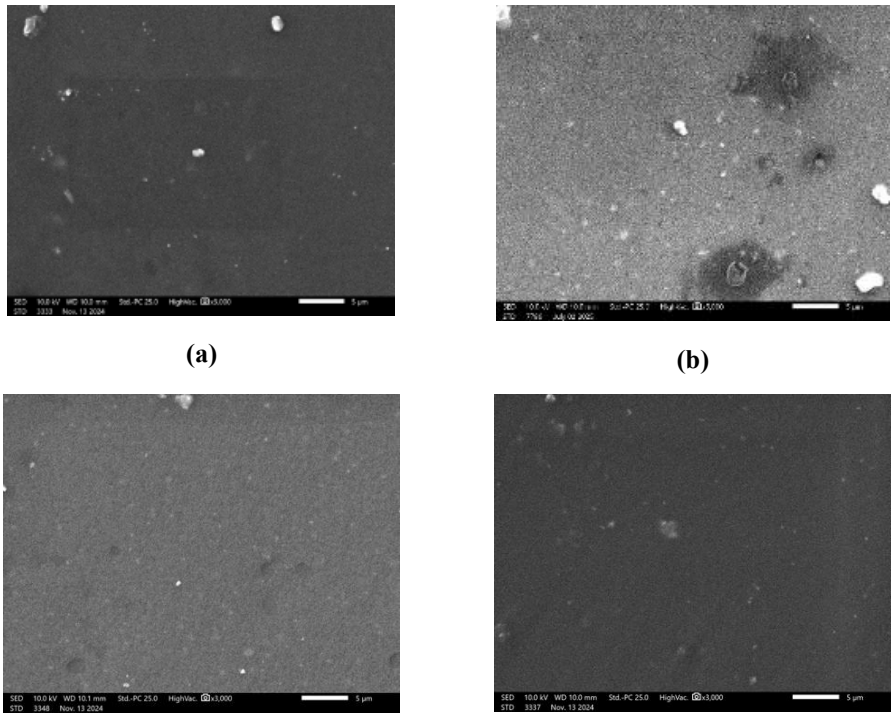

(a) **(b)**

(c) **(d)**

Fig. 2. SEM micrographs of PDMS–CCTO composites at (a) 10 wt.%, (b) 20 wt.%, (c) 40 wt.%, and (d) 60 wt.% ceramic filler loadings.

Table 2. Quantitative SEM analysis of agglomerate size and area fraction for PDMS–CCTO composites.

CCTO Loading (wt.%)	Mean Feret Diameter (µm)	Area Fraction (%)
10	0.51	1.00
20	0.43	0.78
40	0.46	0.72
60	0.53	1.03

Particle dispersion and clustering can be observed with increasing ceramic content. The EDX analysis of CCTO–PDMS composites at different filler loadings is summarized in Table 3. The dominant elements across all samples are carbon

(C), oxygen (O), and silicon (Si), originating from the PDMS matrix. At low filler content (10 wt.% CCTO), the polymer-related elements account for nearly the entire composition, with C at 31.50 ± 0.90 wt.%, O at 27.87 ± 1.05 wt.%, and Si at 38.53 ± 1.35 wt.%. As the CCTO loading increases, the relative fractions of these matrix elements gradually shift. For example, Si increased slightly from 38.53 ± 1.35 wt.% at 10 wt.% to 40.04 ± 1.40 wt.% at 60 wt.%, while C decreased from 31.50 ± 0.90 wt.% to 26.74 ± 0.86 wt.%. Oxygen remained relatively stable (27–31 wt.%), consistent with its presence in both PDMS and CCTO phases.

In contrast, the characteristic elements of CCTO—Ti, Cu, and Ca—become increasingly evident as the filler fraction rises. At 10 wt.% CCTO, only trace amounts of Ti (1.27 ± 0.41 wt.%), Cu (0.42 ± 0.51 wt.%), and Ca (0.41 ± 0.36 wt.%) were detected. At 40 wt.% loading, Ti and Cu increased to 1.04 ± 0.65 wt.% and 1.48 ± 0.45 wt.%, respectively, while Ca remained detectable at 0.31 ± 0.37 wt.%. At the highest loading (60 wt.% CCTO), Ti further increased to 1.52 ± 0.66 wt.% with consistent detection of Cu and Ca, despite minor fluctuations attributed to particle dispersion and the sensitivity limits of EDX.

To complement these quantitative data, Fig. 3 presents a representative EDX spectrum of the composite. The spectrum confirms the presence of the CCTO-related elements (Ca, Cu, Ti) together with the PDMS matrix elements (Si, O), validating the incorporation of the ceramic filler. Since all samples exhibited similar spectral profiles, only one spectrum is presented to avoid repetition, while the detailed compositional variations are summarized in Table 3.

Table 3. Elemental composition of CCTO–PDMS composites at different filler loadings determined by EDX (mass %).

Element	Mass %			
	10wt.% CCTO-PDMS	20wt.% CCTO-PDMS	40wt.% CCTO-PDMS	60 w.% CCTO-PDMS
C	31.50±0.90	33.07±0.40	31.67±0.90	26.74±0.86
O	27.87±1.05	29.80±0.48	27.27±1.05	30.83±1.11
Si	38.53±1.35	36.97±0.58	38.24±1.34	40.04±1.40
Ti	1.27±0.41	0.08±0.18	1.04±0.65	1.52±0.66
Cu	0.42±0.51	0.06±0.14	1.48±0.45	0.71±0.37
Ca	0.41±0.36	0.02±0.12	0.31±0.37	0.15±0.30

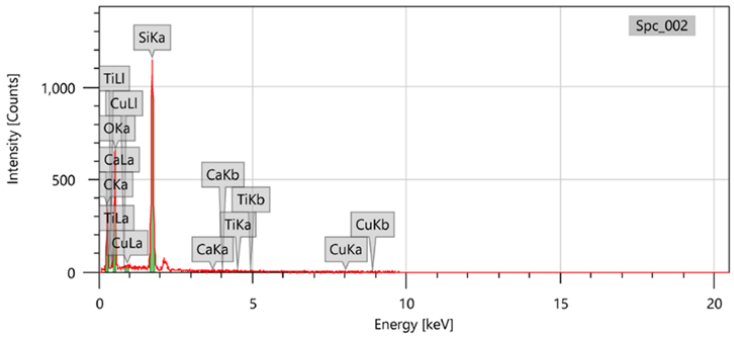

Fig. 3. Representative EDX spectrum of CCTO–PDMS composite showing characteristic ceramic (Ca, Cu, Ti) and polymer (Si, O) elements.

3.2. FTIR characterization of chemical interactions in CCTO–PDMS composites

Figure 4 presents the FTIR spectra of CCTO–PDMS composites fabricated via the solvent casting method, with CCTO incorporated at 10 wt.%, 20 wt.%, 40 wt.%, and 60 wt.%. Across all compositions, the characteristic vibrational bands of PDMS are clearly identifiable, confirming the preservation of the polymer backbone. The absorption peak at 2962.17 cm^{-1} corresponds to symmetric CH_3 stretching, and the band at 1260.75 cm^{-1} arises from Si–CH_3 bending, confirming the preservation of PDMS side groups. The siloxane backbone is evidenced by Si–O–Si stretching at 1086.23 cm^{-1} and 1014.87 cm^{-1}, while the band at 799.84 cm^{-1} is attributed to Si–$(CH_3)_2$ rocking vibrations, consistent with characteristic PDMS spectra [32, 33].

A distinct band at 558.30 cm^{-1} emerges a33nd increases in intensity with higher filler loading, corresponding to the M–O stretching vibrations (Ti–O and Cu–O) originating from the CCTO ceramic phase [34, 35]. This increasing intensity confirms the successful incur poration of CCTO into the PDMS matrix. The absence of new absorption peaks or significant spectral shifts suggests that no chemical bonding or covalent interaction occurs between CCTO and PDMS. This indicates a physically mixed two-phase system, consistent with previous findings on similar ceramic–polymer composites.

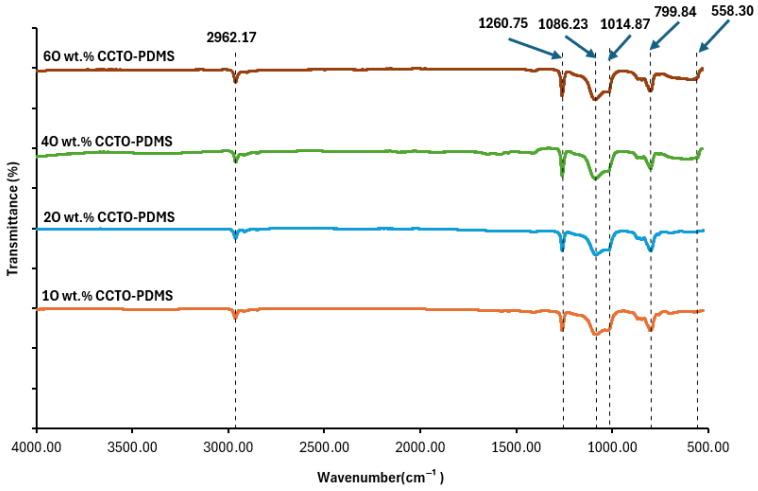

Fig. 4. FTIR spectra of CCTO–PDMS composites formulated with varying ceramic loadings (10–60 wt.%).

3.3. Dielectric Properties and loss tangent

The real and imaginary components of the dielectric constant over the frequency range of 1–10 GHz are shown in Figs. 5(a) and (b), respectively. Pure PDMS is stable and has a low real part of the dielectric constant (ε′), ranging from 2.7--2.8 across the frequency range, which is consistent with its well-known insulating nature. As the CCTO content increased from 10 wt.% to 60 wt.%, a clear increase in ε′ was observed, with the ε′ value of the 60 wt.% CCTO-PDMS sample reaching 6.2 at 6.7 GHz. This increase is attributed to the high intrinsic permittivity of CCTO

($\varepsilon' > 10^4$) and the formation of interfacial polarization zones, which are typically explained by the Maxwell–Wagner–Sillars theory. This variation is typical of frequency-dependent dielectric dispersion in ceramic–polymer composites. A relatively flat frequency response up to 5 GHz is particularly favourable for antenna applications, as stable dielectric behaviour ensures consistent resonance and impedance matching.

The corresponding imaginary part of the dielectric constant (ε''), shown in Fig. 5(b), also increases with increasing CCTO loading. Although ε'' remains relatively low for all compositions, a noticeable peak is observed at 7.5 GHz for the 60 wt.% sample, indicating more pronounced dielectric relaxation at higher filler contents. This behaviour suggests increased interfacial interaction and energy dissipation mechanisms at elevated frequencies.

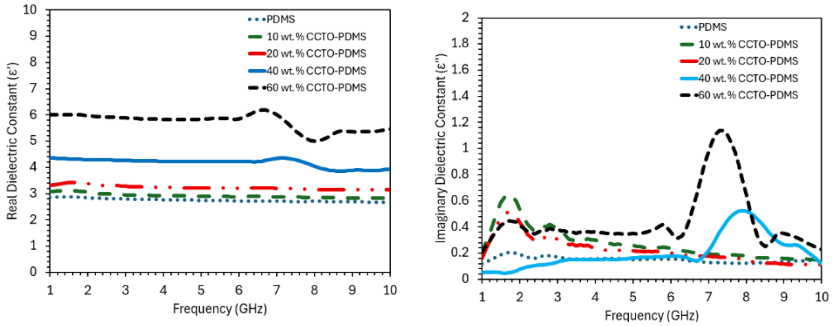

(a) **(b)**

Fig. 5. Dielectric constant (ε') versus frequency for CCTO-PDMS composites (a) Real part (b) Imaginary part.

Figure 6. shows the dielectric loss tangent ($\tan\delta$) of CCTO-PDMS composites measured over the frequency range of 1–10 GHz. In microstrip patch antenna applications, a low $\tan\delta$ is desirable to reduce dielectric losses and improve radiation efficiency. As expected, pure PDMS exhibits stable and has low losses ranging from 0.01 to 0.08 because of its minimal polarization mechanisms. With the introduction of CCTO, the loss behaviour becomes more complex. At 10 wt.%, a broad peak appears at approximately 2 GHz, suggesting poor dispersion and unstable interfacial polarization. Interestingly, the 20 wt.% sample demonstrated slightly reduced loss, indicating some improvement in filler distribution. The 40 wt.% composition is the most stable and has the lowest overall loss, maintaining $\tan\delta$ values below 0.07 across the full frequency range. This implies a well-dispersed ceramic–polymer network that enhances the permittivity without introducing excessive relaxation losses.

In contrast, the 60 wt.% sample exhibited a distinct peak at 0.20 near 7.5 GHz. This sharp rise is likely due to filler–filler interactions and agglomeration at higher loading levels, which increases interfacial polarization and conduction losses. However, this composition also delivers the highest dielectric constant, making it a valuable candidate for compact antenna design where miniaturization and high field confinement are key. Although its dielectric loss is relatively high, it remains within acceptable limits for GHz-range applications. Thus, the 60 wt.% CCTO-

PDMS composite offers a better trade-off with a higher dielectric constant at the cost of moderately increased losses, making it suitable for high-performance, flexible antenna substrates.

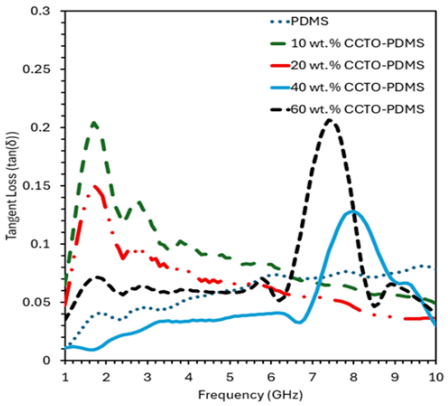

Fig. 6. Dielectric loss tangent (tan δ) vs. frequency for CCTO-PDMS composites

Figures 7 and 8 present the dielectric properties of CCTO-PDMS composites measured at 5.2 GHz, a frequency relevant to second-band wireless communication applications. The real part of the dielectric constant (ε′) increases steadily with filler loading, reaching a peak value of 5.84 at 60 wt.%. This enhancement is advantageous for microstrip patch antenna (MPA) designs, where higher ε′ allows for reduced antenna dimensions and improved field confinement. The slight variation between the dielectric constant measured at 6.7 GHz and the value reported at 5.2 GHz arises from frequency-dependent dielectric dispersion. In ceramic–polymer composites, permittivity may vary with frequency due to interfacial polarization, dipolar relaxation, and localized charge accumulation at filler–matrix interfaces. Therefore, the value of 6.2 at 6.7 GHz and 5.84 at 5.2 GHz are consistent and reflect the normal dielectric response of heterogeneous composites across the microwave frequency range.

Although the tangent loss (tan δ) at 60 wt.% is moderately higher than at lower filler ratios, it remains within a tolerable range for many GHz-range applications, especially where size reduction and gain optimization are prioritized. The high dielectric performance of the 60 wt.% composite is further supported by SEM observations, which reveal a relatively well-dispersed filler distribution with only minor agglomeration. Despite some particle clustering, no continuous conductive pathways are formed, indicating that interfacial polarization is controlled and dielectric losses are manageable.

Therefore, among all tested formulations, the 60 wt.% CCTO-PDMS composite demonstrated the most promising dielectric profile for GHz-frequency applications. This approach provides a strong balance between elevated permittivity and acceptable loss, making it an ideal candidate for next-generation flexible MPA substrates aimed at compact and high-efficiency wireless systems.

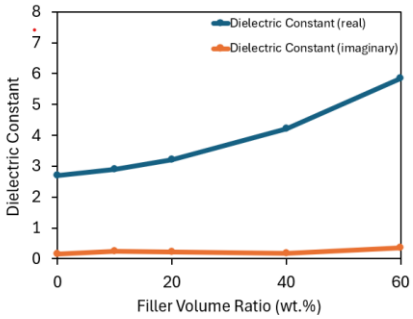

Fig. 7. Real part of the dielectric constant (ε′) at 5.2 GHz versus filler volume ratio in CCTO-PDMS composites.

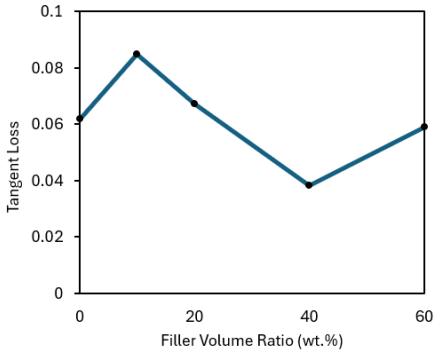

Fig. 8. Dielectric loss tangent (tan δ) at 5.2 GHz vs. filler volume ratio in CCTO-PDMS composites.

3.4. Comparison of dielectric mixing models with experimental validation

Figure 9 compares the experimental dielectric response of CCTO–PDMS composites with several classical mixing models. The measured permittivity increases progressively with increasing filler content, showing a moderate enhancement up to 25 vol.%. Among the theoretical predictions, the Maxwell–Garnett and Jayasundere–Smith models exhibit the closest agreement with the experimental trend across the investigated range. This indicates that both models reasonably describe the effective medium behaviour at dilute to intermediate filler concentrations, where dielectric response is primarily governed by localized particle–matrix interactions rather than long-range filler connectivity.

In contrast, the Lichtenecker logarithmic model significantly overestimates the effective permittivity, particularly beyond 15 vol.% loading. This deviation arises from its assumption of an idealized uniform field distribution without considering the limited dispersion and non-percolative nature of ceramic fillers in the elastomeric PDMS matrix. Similarly, the symmetric Bruggeman approximation predicts higher values at larger filler fractions, reflecting its inherent sensitivity to percolative tendencies. These discrepancies highlight that while such models provide useful theoretical bounds, they do not fully capture microstructural factors such as partial agglomeration, interfacial heterogeneity, or constrained dipolar relaxation within flexible matrices.

The close agreement between the experimental data and the Maxwell–Garnett prediction reflects the microstructural characteristics of the present composite system. Although compositions are reported in weight percentage (wt.%) for fabrication consistency, the model was implemented using the corresponding volume fractions calculated from the measured material densities. The Maxwell–Garnett formulation assumes discrete inclusions embedded in a continuous host matrix under non-percolative conditions. Morphological observations confirm relatively uniform particle dispersion within the PDMS matrix across 10–60 wt.% loading, supporting the validity of this effective medium assumption. The monotonic increase in permittivity and the absence of abrupt dielectric transitions further indicate that the composite remains below the percolation regime. Within this range, the Maxwell–Garnett approach provides a physically consistent and reliable prediction of effective permittivity, despite not explicitly accounting for particle interactions or interfacial imperfections at higher loadings.

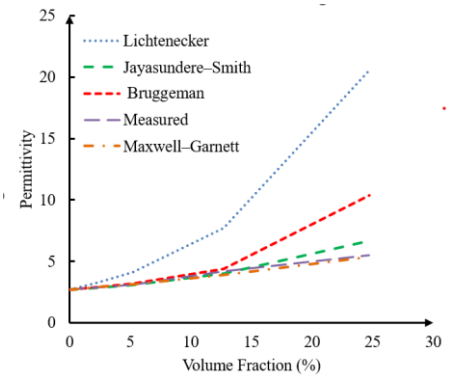

Fig. 9. Comparison of measured and theoretical permittivity of CCTO–PDMS composites versus volume fraction.

3.5. Comparative analysis with previous works

To evaluate the performance of the developed CCTO–PDMS composites in a broader context, a comparative summary of dielectric permittivity (εr) from selected CCTO-based polymer systems is presented in Table 4. The reported values vary considerably with filler loading, polymer matrix, and, most critically, measurement frequency.

For instance, a 50 vol.% CCTO–PVDF composite exhibits a dielectric constant of 52 measured within the 10^2–10^6 Hz range [44]. Likewise, a 20 wt.% CCTO–PDMS composite measured at 100 Hz reports $\varepsilon r \approx 5.8$ [45], and a 25 wt.% CCTO–silicone rubber system shows εr values between 5.14 and 5.04 across 10^2–10^6 Hz [46]. It is important to emphasize that all these reported values were obtained in the low-frequency regime (Hz to kHz range), whereas the present work evaluates dielectric performance at microwave frequencies, specifically 1.1 GHz and 5.2 GHz.

This distinction is fundamental. In ceramic–polymer composites, dielectric permittivity at low frequencies is strongly influenced by interfacial polarization, where charge carriers accumulate at filler–matrix interfaces and significantly enhance the apparent εr. At microwave frequencies in the GHz range, however, the electric field oscillates too rapidly for space charges to respond effectively. As a

result, the contribution of Maxwell–Wagner–Sillars polarization diminishes, and the dielectric response becomes dominated by intrinsic electronic and ionic polarization mechanisms. Consequently, εr values measured at 100 Hz or within 10^2–10^6 Hz cannot be directly compared with those obtained at GHz frequencies without considering polarization relaxation effects.

The trends observed in Table 4 are consistent with the frequency-dependent polarization behaviour commonly reported for ceramic–polymer composites. In heterogeneous systems such as CCTO–PDMS, the dielectric response arises from electronic, ionic, dipolar, and interfacial (Maxwell–Wagner–Sillars, MWS) polarization mechanisms. At low frequencies, interfacial polarization dominates because charge carriers have sufficient time to accumulate at ceramic–polymer interfaces, leading to enhanced apparent permittivity [36, 37]. As the frequency increases into the MHz and GHz ranges, the electric field alternates too rapidly for interfacial charges to respond effectively. Consequently, the contribution of MWS polarization diminishes, and the dielectric behaviour becomes governed primarily by intrinsic electronic and ionic polarization processes [37, 38]. Similar relaxation behaviour has been reported for CCTO-based polymer composites, where εr decreases with increasing frequency due to reduced interfacial charge mobility [39], while conductivity–polarization scaling further supports the weakening of space-charge effects at elevated frequencies [40].

This mechanism is reflected in the present CCTO–PDMS composites. For the 60 wt.% sample, εr decreases slightly from 6.01 at 1.1 GHz to 5.84 at 5.2 GHz, consistent with polarization relaxation under microwave excitation rather than structural degradation. Increasing the CCTO loading from 10 to 60 wt.% increases the density of ceramic–polymer interfaces and polarization sites, resulting in a monotonic enhancement of εr even at 5.2 GHz. The absence of abrupt dielectric dispersion suggests that the composite remains below the percolation threshold and does not form continuous conductive pathways. Therefore, differences among studies in Table 4 should be interpreted primarily in terms of measurement frequency and polarization dynamics rather than composition alone. The εr value of 5.84 at 5.2 GHz is consistent with the intrinsic high-frequency dielectric response expected for CCTO-based composites designed for microwave antenna applications.

Table 4. Comparative summary of dielectric permittivity values for CCTO-based polymer composites reported in the literature and the present work.

Composite	Frequency	Dielectric Constant	Ref.
CCTO 60 wt.% +PDMS	1.1 GHz (microwave frequency)	6.01	**This work**
CCTO 60 wt.% +PDMS	5.2 GHz (microwave frequency)	5.84	**This work**
CCTO 50 vol .% + PVDF	10^2 Hz to 10^6 Hz	5.2	[41]
CCTO 20 wt.% + PDMS	100 Hz	5.8	[42]
CCTO 25 wt.% + Silicone Rubber	10^2 to 10^6 Hz.	5.14 to 5.04	[43]

3.6. Materials and methods justification

The selection of CCTO as the ceramic filler is motivated by its intrinsically high dielectric constant, which enables effective permittivity enhancement at relatively moderate filler loading compared to conventional ceramic additives. PDMS was chosen as the polymer matrix due to its excellent mechanical flexibility, low intrinsic dielectric loss at microwave frequencies, ease of processing, and suitability for wearable and conformal electronics. The solvent-assisted dispersion approach using isopropanol was adopted to improve filler distribution and reduce agglomeration, which is critical for achieving stable dielectric properties in heterogeneous composites.

In this study, it is assumed that the CCTO particles are physically dispersed within the PDMS matrix without significant chemical bonding, as supported by FTIR analysis. The dielectric characterization further assumes effective medium behaviour, where the composite response is governed by interfacial polarization and filler–matrix interactions rather than long-range conductive pathways. Nevertheless, several limitations must be acknowledged. At high filler loading, increased dielectric loss may arise due to localized charge accumulation and partial percolation effects. Furthermore, the dielectric properties reported at microwave frequencies may exhibit dispersion when compared with low-frequency measurements, limiting direct comparison with literature values obtained under different testing conditions. These considerations define the scope and applicability of the proposed material system.

4. Conclusion

Flexible CCTO–PDMS composites with ceramic loadings from 10 to 60 wt.% were successfully fabricated and evaluated as dielectric substrates for microwave applications. Morphological and spectroscopic analyses confirmed uniform particle dispersion within the elastomeric matrix without chemical interaction, supporting the formation of a stable two-phase composite structure. Dielectric measurements at 5.2 GHz revealed a systematic increase in permittivity with filler loading, reaching 5.84 at 60 wt.% while maintaining acceptable dielectric loss. The experimental results showed good agreement with the Maxwell–Garnett effective medium model at low to moderate filler fractions, demonstrating its suitability for predicting the dielectric behaviour of the composite system. Deviations at higher loadings were attributed to particle clustering and interfacial polarization effects.

Overall, the developed CCTO–PDMS composite provides a balanced combination of enhanced permittivity, structural flexibility, and fabrication simplicity, making it a promising candidate for flexible RF substrates and wearable antenna platforms. Future work will focus on evaluating the mechanical properties of the developed composites, including tensile and bending performance, to confirm their structural reliability as flexible antenna substrates. In addition, the composite will be integrated into a microstrip patch antenna prototype to assess electromagnetic performance under bending conditions. Key antenna parameters such as resonance stability, return loss, bandwidth, gain, and radiation efficiency will be investigated to validate practical applicability in flexible RF systems.

Acknowledgement

This work has been supported by the Ministry of Higher Education Malaysia (MoHE) FRGS grant FRGS/1/2024/TK09/UMP/03/1 (RDU240105) and Universiti Malaysia Pahang Al-Sultan Abdullah (UMPSA). Their involvement enabled the successful completion of our research at the UMPSA STEM Lab, the Faculty of Electrical and Electronics Engineering Technology, UMPSA.

References

1. Omer, H.A.H.; Azemi, S.N.; Al-Hadi, A.A.; Soh, P.J.; and Jamlos, M.F. (2018). Structural health monitoring sensor based on a flexible microstrip patch antenna. *Indonesian Journal of Electrical Engineering and Computer Science*, 10(3), 917–924.
2. Salleh, S.M.; Ain, M.F.; Ahmad, Z.; Abidin, I.S.Z.; Seng, L.Y.; and Osman, M.N. (2023). Stretchable and bendable polydimethylsiloxane-silver composite antenna on PDMS/Air gap substrate for 5G wearable applications. *IEEE Access*, 11,133623-133639.
3. Sharma, A.; and Kumar, P. (2022). Design of a flexible microstrip antenna for BAN applications. *Journal of Physics: Conference Series*, 2161, 012012.
4. Ju, L.; Yu, B.-Y.; Geng, M.-Y.; and Lu, W.-B. (2024). Stretchable and miniaturized backscatter antenna based on serpentine metallic structures and PDMS-$BaTiO_3$ composite. *Proceedings of the 2024 International Conference on Electrical, Computer and Energy Technologies (ICECET)*, Sydney, Australia, 1-3.
5. Thiruramanathan, P.; Marikani, A.; Ravi, S.; Madhavan, D.; and Hikku, G.S. (2018). Fabrication of miniaturized high bandwidth dielectric resonator on patch (DRoP) antenna using high dielectric $CaCu_3Ti_4O_{12}$ nanoparticles. *Journal of Alloys and Compounds*, 747, 1033-1042.
6. Katzmarek, D.A.; Pradeepkumar, A.; Ziolkowski, R.W.; Al-Haddad, M.; Jamel, N.; and Nordin, A.N. (2021). Flexible antenna: A review of design, materials, fabrication, and applications. *Journal of Physics: Conference Series*, 1878(1), 012068.
7. John, D.M.; Vincent, S.; Pathan, S.; Kumar, P.; and Ali, T. (2022). Flexible antennas for a sub-6 GHz 5G band: A comprehensive review. *Sensors*, 22(19), 7615.
8. Chang, X.L.; Chee, P.S.; and Lim, E.H. (2023). Compact conformal tattoo-polymer antenna for on-body wireless power transfer. *Scientific Reports*, 13(1), 9678.
9. Khan, S.; Mazhar, T.; Shahzad, T.; Bibi, A.; Ahmad, W.; Khan, M.A.; Saeed, M.M.; and Hamam, H. (2024). Antenna systems for IoT applications: A review. *Discover Sustainability*, 5(1), 412.
10. Panda, S.; Gupta, A.; and Acharya, B. (2019). Wearable microstrip patch antennas with different flexible substrates for health monitoring system. *Materials Today: Proceedings*, 45(Part 4), 4002-4007.
11. Abbas, S.M.; Desai, S.C.; Esselle, K.P.; Volakis, J.L.; and Hashmi, R.M. (2018). Design and characterization of a flexible wideband antenna using

polydimethylsiloxane composite substrate. *International Journal of Antennas and Propagation*, Article ID 4095765.

12. Sharma, P.K.; and Chung, J.-Y. (2023). Evaluation of polydimethylsiloxane (PDMS) as a substrate for the realization of flexible/wearable antennas and sensors. *Micromachines*, 14(4), 735.
13. Rana, D.K.; Banerjee, P.S.; Betal, S.; and Banerjee, S.S. (2023). Ultra-stretchable thermoplastic elastomeric materials based on styrene–isoprene–styrene triblock copolymer: Influence of calcium copper titanate on mechanical and dielectric properties. *Journal of Applied Polymer Science*, 141(4), e54857.
14. Gobiraman, A.; Nagaraja, S.; and Sathiyamoorthi, V. (2023). *Epoxy resin as matrix for polymer composites: Factors influencing the properties of polymers and their composites*. In Muthukumar, C.; Muthu Kumar Thiagamani, S.; Krishnasamy, S.; and Bin Rushdan, A.I. (Eds.). *Epoxy-Based Biocomposites*. CRC Press, Boca Raton, 1–19.
15. Wei, H.; Wang, D.; and Xing, W. (2023). Strengthening and toughening technology of epoxy resin. *Journal of Physics: Conference Series*, 2468, 012066.
16. Khan, M.S. (2023). The tribological characteristic of wear in alloy steel composite material. *International Journal of Scientific Research in Engineering and Management*, 7(8).
17. Imah Luluk, K.; Putu Arta Wibawa, I.; Gafur, A.; Widodo, E.W.R.; Dianita, W.; Tamimah, N.; Sumardiono; Agung, P.U.; Abdullah, K.; and Dhiya Anissa, U. (2023). Analysis of adhesive strength of epoxy DGEBA on the wooden boat hull. *IOP Conference Series: Earth and Environmental Science*, 1265, 012021.
18. Mohanty, D.; Mohanty, S.; and Kanny, K. (2025). *Role of additives in waterborne epoxy coatings*. In Pradhan, S.; Moharana, S.; and Mohanty, S. (Eds.). *Recent advances on waterborne epoxy coatings. Materials horizons: From nature to nanomaterials*. Springer, Singapore. Part F449, 37-62.
19. Munard Diaz, M.S.; Sanchez Duran, S.M.; and Sanchez Londono, Y.A. (2024). Ecotoxicity in Teflon's life cycle. *Proceedings of the Congreso Internacional de Innovación y Tendencias en Ingeniería (CONIITI).* , Bogotá, Colombia, 2024, 1-4,
20. Roslan, R.A; Noordin, N.H.; Hasan, N.; Naharuddin N.Z.A.B.; and Mohd Radi N.H. (2026). Influence of solvent and non-solvent fabrication techniques on the properties of CCTO-PDMS composites. *Journal of Engineering Science and Technology*, 21(2), 495-511.
21. Wang, W.; Ren, G.; Zhou, M.; and Deng, W. (2021). Preparation and characterization of CCTO/PDMS dielectric elastomers with high dielectric constant and low dielectric loss. *Polymers*, 13(7), 1075.
22. Liu, G.; Chen, Y.; Gong, M.; Liu, X.; Cui, Z.K.; Pei, Q.; Gu, J.; Huang, C.; and Zhuang, Q. (2018). Enhanced dielectric performance of PDMS-based three-phase percolative nanocomposite films incorporating a high dielectric constant ceramic and conductive multi-walled carbon nanotubes. *Journal of Materials Chemistry C*, 6(4), 10829-10837.
23. Xinyu, D.; Shi, L.; Xinyue, H.; and Zhang, T. (2024). Microwave dielectric properties calculation of Si_2N_2O/BN composites based on mixture equations.

Proceedings of the IEEE International Conference on Emerging Technologies (ICET), Chengdu, China, 290–294.

24. Chahinaz, A.; Nacerdine, B.; Abdelhalim, B.; Habib, K.; and Sabrine, T. (2024). Comparative study between Lichtenecker modified model and Bottreau's law for two binary composites (RE-BT) and (RE-SiO_2). *Proceedings of the 2024 International Conference on Advances in Electrical and Communication Technologies (ICAECOT)*, Setif, Algeria, 2024, 1-7.
25. Shan, Y.; Lu, Y.; and Zhou, H. (2024). Investigation on phase composition and microwave dielectric properties of MgO-SiO_2-TiO_2 system. *Journal of Materials Science: Materials in Electronics*, 35(14), 979.
26. Brandt, J.; Dittrich, G.; Renner, H.; Huber, P.; Eich, M.; and Petrov, A. (2024). On the applicability of the Maxwell Garnett effective medium model to media with a high density of cylindrical pores. *Optical Materials Express*, 14(4), 871-879.
27. Kalandadze, L.; Nakashidze, O.; Gomidze, N.; and Jabnidze, I. (2024). On the effective permittivity of the multicomponent dielectric-dielectric nanocomposite structures. *AIP Conference Proceedings*, 3149, 0224569.
28. Zhao, T.; Zeng, T.; Jin, S.; Li, X.; and Yu, Z. (2025). Sol-gel prepared BNST-Mn ceramics and its PTFE composites: Synthesis and performance analysis. *Journal of Materials Science: Materials in Electronics*, 36(14), 831.
29. Han, R.; Ren, J.; Quan, H.; Wang, X.; Qi, W.; Gao, D.; Zhou, Z.; Li, Q.; and Chen, G.-X. (2024). Construction of parallel-structured composites based on a theoretical model to achieve an ultra-high dielectric constant. *Journal of Materials Chemistry A*, 12(34), 22785-22796.
30. Keshyagol, K.; Hiremath, S.; Vishwanatha, H.M.; Rao, P.K.; Hiremath, P.; and Naik, N. (2024). Analysis of polymer-ceramic composites performance on electrical and mechanical properties through finite element and empirical models. *Materials*, 17(15), 3837.
31. Madhu, B.M.; Aradhya, R.; and Suma, P. (2025). Thermal aging analysis and predictive modeling of epoxy nanocomposites characteristics. *Journal of Vinyl and Additive Technology*, 32(1), 55-64.
32. Vazirinasab, E. (2020). *Superhydrophobic silicone-based nanocomposites for application to high voltage insulator*. Ph.D. Thesis, Université du Québec à Chicoutimi (UQAC), Canada.
33. Mikolaszek, B.; Jamrógiewicz, M.; Mojsiewicz-Pieńkowska, K.; and Sznitowska, M. (2022). Microscopic and spectroscopic imaging and thermal analysis of acrylates, silicones and active pharmaceutical ingredients in adhesive transdermal patches. *Polymers*, 14(14), 2888.
34. Jesurani, S.; Kanagesan, S.; Velmurugan, R.; and Kalaivani, T. (2012). Phase formation and high dielectric constant of calcium copper titanate using sol-gel route. *Journal of Materials Science: Materials in Electronics*, 23(3), 668-674.
35. Hadi, N.; Abdi, F.; Lamcharfi, T.; Belaaraj, A.; Kassou, S.; and Ahjyaje, F. (2019). Study of the dielectric, optical and microstructure properties of $CaCu_3Ti_4O_{12}$-$PbZr_{0.48}Ti_{0.52}O_3$ ceramic system with different compositions. *Mediterranean Journal of Chemistry*, 8(3), 245.
36. Drakopoulos, S.X.; Cui, J.; Asandulesa, M.; Blom, P.W.M.; Nogales, A.; and Asadi, K. (2024). Universal scaling of DC conductivity with dielectric interfacial polarization in conjugated polymers. *Macromolecules*, 57(6), 2661-2668.

37. Bronnikov, S.; Kostromin, S.; Asandulesa, M.; Pankin, D.; and Podshivalov, A. (2020). Interfacial interactions and interfacial polarization in polyazomethine/MWCNTs nanocomposites. *Composites Science and Technology*, 190, 108049.
38. Dias, C.J.; Igreja, R.; Marat-Mendes, R.; Inácio, P.; Marat-Mendes, J.N.; and Das-Gupta, D.K. (2004). Recent advances in ceramic-polymer composite electrets. *IEEE Transactions on Dielectrics and Electrical Insulation*, 11(1), 35-40.
39. Mishra, S.; Mishra, P.; Mohapatra, D.K.; Mishra, P.; Mishra, D.K.; and Shadangi, K.P. (2024). Study of frequency dependence properties of CCTO-BT/polymer composites. *Proceedings of the Institution of Mechanical Engineers, Part C: Journal of Mechanical Engineering Science*, 238(6), 2140-2149.
40. Pandey, J.C.; and Singh, M. (2021). Dielectric polymer nanocomposites: Past advances and future prospects in electrical insulation perspective. *SPE Polymers*, 2(4), 236-256.
41. Wang, J.J.; Deng, Q.J.; He, Y.Y.; Feng, Y.N.; Kang, M.P.; Duan, X.L.; and Yang, Y.L. (2022). Fabrications and dielectric performances of novel composites: Calcium copper titanate/polyvinylidene fluoride. *Current Applied Physics*, 39, 25-29.
42. Mihara, S.; and Takeoka, S. (2022). Preparation and characterization of highly elongated polydimethylsiloxane nanosheets. *Polymer Advanced Technologies*, 33(4), 1180-1189.
43. Radzivilov, E.; Zotov, I.; Vikulova, M.; Tsyganov, A.; Artyukhov, I.; Artyukhov, D.; Gorokhovsky, A.; Yudin, A.; and Gorshkov, N. (2025). High-permittivity silicone composites with different polarization titanates for electric field modification. *Polymers*, 17(7), 986.